Rogozhina, I., Petrunin, A. G., Vaughan, A. P. M., Steinberger, B., Johnson, J. V., Kaban, M. K., Calov, R., Rickers, F., Thomas, M., Koulakov, I. (2016): Melting at the base of the Greenland Ice Sheet explained by Iceland hotspot history.- *Nature Geoscience*, *9*, pp. 366–369.

DOI: http://doi.org/10.1038/ngeo2689

# Melting at the base of the Greenland Ice Sheet explained by Iceland hotspot history

**Authors:** Irina Rogozhina[1,2], Alexey G. Petrunin[3,1,4], Alan P. M. Vaughan[5,6], Bernhard Steinberger[1,7], Jesse V. Johnson[8], Mikhail K. Kaban[1,4], Reinhard Calov[9], Florian Rickers[10], Maik Thomas[1,11], Ivan Koulakov[12,13]

[1] Helmholtz Centre Potsdam GFZ German Research Centre For Geosciences, Potsdam, Germany

[2] Center for Marine Environmental Sciences, University of Bremen, Bremen, Germany

[3] Faculty of Earth Sciences, Goethe University, Frankfurt am Main, Germany

[4] Schmidt Institute of Physics of the Earth, Moscow, Russia

[5] Midland Valley Exploration Ltd, Glasgow, United Kingdom

[6] Department of Geology, Trinity College, Dublin 2, Ireland

[7] Centre for Earth Evolution and Dynamics (CEED), University of Oslo, Oslo, Norway

[8] Department of Computer Science, The University of Montana, Missoula, United States of America

[9] Potsdam Institute for Climate Impact Research (PIK), Potsdam, Germany

[10] Department of Earth Sciences, Utrecht University, Utrecht, The Netherlands

[11] Berlin Free University, Institute of Meteorology, Faculty of Geosciences, Berlin, Germany

[12] Institute of Petroleum Geology and Geophysics, Novosibirsk, Russia

[13] Geological Department, Novosibirsk State University, Novosibirsk, Russia

I. Rogozhina*

Helmholtz Centre Potsdam, GFZ German Research Centre for Geosciences, Section 1.3: Earth System Modelling, Telegrafenberg A20, D-14473 Potsdam, Germany

Center for Marine Environmental Sciences, University of Bremen, Klagenfurter str. 2, D-28359 Bremen, Germany

Phone: +49 (0) 421 218 65433, Fax: +49 (0) 331 288 1163, email: irogozhina@marum.de

A. G. Petrunin
Goethe University, Faculty of Earth Sciences, Section Geophysics, Altenhöferallee 1, 60323 Frankfurt am Main, Germany
Helmholtz Centre Potsdam, GFZ German Research Centre for Geosciences, Section 1.3: Earth System Modelling, Telegrafenberg A20, D-14473 Potsdam, Germany
Schmidt Institute of Physics of the Earth, B. Gruzinskaya 10, 123995 Moscow, Russia
Phone: +49 (0) 331 288 1930, Fax: +49 (0) 331 288 163, email: alexei@gfz-potsdam.de

A. P. M. Vaughan
Midland Valley Exploration Ltd, 2 West Regent St, Glasgow, G2 1RW, United Kingdom
Trinity College, Department of Geology, Dublin 2, Ireland
Phone: +44 (0) 141 332 2681, Fax : +44 (0) 141 332 6792, email: avaughan@mve.com

B. Steinberger
Helmholtz Centre Potsdam, GFZ German Research Centre for Geosciences, Section 2.5: Geodynamic Modelling, Heinrich-Mann-Allee 18/19, D-14473 Potsdam, Germany
Centre for Earth Evolution and Dynamics (CEED), University of Oslo, P.O. Box 1048, Blindern, 0316 Oslo, Norway
Phone: +49 (0) 331 288 1881, Fax: +49 (0) 331 288 1938, email: bstein@gfz-potsdam.de

J. V. Johnson
The University of Montana, Department of Computer Science, Missoula, MT 59812-5256, United States of America
Phone: (406) 243-2356, Fax: (406) 243-5139, email: jesse.johnson@mso.umt.edu

M. K. Kaban
Helmholtz Centre Potsdam, GFZ German Research Centre for Geosciences, Section 1.3: Earth System Modelling, Telegrafenberg A20, D-14473 Potsdam, Germany
Schmidt Institute of Physics of the Earth, B. Gruzinskaya 10, 123995 Moscow, Russia
Phone: +49 (0) 331 288 1172, Fax: +49 (0) 331 288 1163, email: kaban@gfz-potsdam.de

R. Calov
Potsdam Institute for Climate Research (PIK), Postfach 60 12 03, D-14412 Potsdam, Germany
Phone: +49 (0) 331 288-2595, email: calov@pik-potsdam.de

F. Rickers
Department of Earth Sciences, Utrecht University, Budapestlaan 4, 3584 CD, Utrecht, The Netherlands
Phone: +33 (0) 183 95-7541, email: florian.rickers@gmail.com

M. Thomas
Helmholtz Centre Potsdam, GFZ German Research Centre for Geosciences, Section 1.3: Earth System Modelling, Telegrafenberg A20, D-14473 Potsdam, Germany
Berlin Free University, Institute of Meteorology, Faculty of Geosciences, Carl-Heinrich-Becker-Weg 6-10, 12165 Berlin, Germany
Phone: +49 (0) 331 288 1147, Fax: +49 (0) 331 288 1163, email: mthomas@gfz-potsdam.de

I. Koulakov
Institute of Petroleum Geology and Geophysics, SB RAS, Novosibirsk, 3, Prospekt Koptyuga, 630090 Novosibirsk, Russia
Geological Department, Novosibirsk State University, Pirogova Str. 2, 630090 Novosibirsk, Russia
Phone: +7 383 3309201, email: KoulakovIY@ipgg.nsc.ru

Correspondence to: I. Rogozhina, email: irogozhina@marum.de

**Ice-penetrating radar[1-3] and ice core drilling[4] have shown that large parts of the north-central Greenland Ice Sheet are melting from below. It has been argued that basal ice melt is sourced from the anomalously high geothermal flux[1,4] that has also influenced the development of the longest ice stream in Greenland[1]. Here we estimate geothermal flux beneath the Greenland Ice Sheet and identify a 1200-km-long and 400-km-wide geothermal anomaly beneath the thick ice cover. We suggest this anomaly explains the observed melting of the ice sheet's base, which drives vigorous subglacial hydrology[3] and controls the position of the head of the enigmatic 750-km-long north-eastern Greenland ice stream[5]. Our joint analysis of independent seismic, gravity and tectonic data[6-9] implies that the geothermal anomaly, which crosses Greenland from west to east, was formed by Greenland's passage over the Iceland mantle plume between approximately 80 and 35 million years ago. This study shows that the complexity of the present-day subglacial hydrology and dynamic features of the north-central Greenland Ice Sheet originated in tectonic events that predate the onset of Greenland glaciations by many tens of millions of years.**

Recent observations indicate that strong regional variations in geothermal flux (GF) dominate the thermal regime and melting of the ice base beneath continental parts of the Greenland and Antarctic ice sheets[1,10]. Ice flows rapidly and subglacial hydrological systems develop where GF is high and melt water is present under ice cover[11-12]. Despite being small compared to the observed volumes of water discharged by surface melt[13], GF-induced basal melt is important because it occurs over large areas in the accumulation zone where there are no other basal water sources, and disproportionately affects the overall dynamic behavior of large ice sheet sectors[1,14].

Deep ice core measurements and data from airborne ice-penetrating radar support very high rates of basal melt for parts of the Greenland Ice Sheet (GIS)[1,4], for example, at the head of the longest ice stream in Greenland, which drains north-east from the summit dome[1]. It has been argued that anomalously high GF, exceeding 100 mW/m$^2$, is required to produce estimated rates of basal melt in the north-central GIS[1,4]. These values significantly exceed those expected for ancient continental crust[15], i.e. 37 to 50 mW/m$^2$, which forms the center of the Greenland craton. Here we present a new reconstruction of GF across north-central Greenland to explain the origin of the observed melting beneath the ice cover (Figure 1). This reconstruction reconciles a large array of independent data sets through an iterative calibration of a coupled 3-D climate-forced model of the GIS and the underlying lithosphere[16] against (i) Curie depths (580ºC isotherm) from satellite magnetic data[17], (ii) estimates of lithosphere thickness from seismic data[18], (iii) bedrock borehole temperature measurements taken in eastern Greenland and at the continental shelf, (iv) ice temperature measurements from five deep ice cores[19], (v) areas of basal ice melt inferred from ice-penetrating radar studies[1-3], (vi) areas of increased ice surface velocity from satellite observations[4], and (vii) measured ice thickness[20] (see Methods).

The reconstructed GF values range from 37 to 106 mW/m$^2$ and show a continuous area of elevated GF (75 – 106 mW/m$^2$) running from Scoresby Sund in the southeast, towards near Melville Bugt in northwest Greenland (Figure 1). The GF in the zone of anomalously high values, although elevated relative to values expected for Precambrian Greenland crust, is lower than previous estimates[1,4], which were in the range 98 to 970 mW/m$^2$. These earlier GF estimates were derived from inferred basal melt rates, which may locally be modulated by factors independent of the solid Earth-sourced heat flux. Sources of significant local perturbations to basal melt rates are: heat advection through subglacial hydrology or hydrothermal circulation, basal ice sliding and meltwater refreezing. Because melting rates are controlled by a combination of GF and non-GF influences, we build our calibration strategy on estimating GF required to reproduce the observed thawed basal ice conditions, discounting basal ice melt rates as a proxy for GF. This has the effect that GF estimates will likely be biased downwards where basal melt is rapid; nevertheless, our strategy is sufficiently effective to separate out the signal of a strong and spatially extensive geothermal anomaly beneath the GIS and provides a hard lower bound for GF values at the observed basal melt locations.

The anomalous GF zone lies in the area with the highest density of direct measurements. These include two deep ice cores (NGRIP and NEEM) and radar soundings at the heart of the anomaly (Figure 1). Three other ice cores (CC, GRIP and GISP2) bound the anomaly to the west and south. The lateral dimensions of the reconstructed geothermal anomaly are roughly 1200 by 400 km, covering about a quarter of the Greenland land area. GF values in the anomalous area are up to 2.5 times background GF values derived across the northern and western parts of Greenland.

One potential cause of elevated GF is illustrated by seismic data that link our west-to-east GF anomaly with a zone of low-seismic-velocity mantle, a "negative anomaly", beneath Iceland[6-7] and Greenland (Figures 1 and 2a-b). Negative anomalies in seismic velocity are commonly associated with anomalously high temperature and compositional heterogeneity of mantle rocks[21]. Iceland has been classified as a geological hotspot interpreted to result from increased magma production attributed to a mantle plume[6,22], which is a narrow zone of hotter than average mantle rock that rises several thousand kilometers from deep within the Earth[23].

Paleoreconstructions of relative plate motion[8-9] and evidence from igneous rocks in eastern and western Greenland[22] suggest that Greenland transited over the Iceland mantle plume between ~80 and 35 million years ago (Figure 2a). When continental lithosphere moves over mantle plumes, compositional and thermal changes, magmatism and lithosphere thinning may affect areas hundreds of kilometers wide[24] (see Supplementary Information). These changes may be independently inferred using anomalies in the observed gravity field (Figure S6), seismic velocity (Figures 2a-b) observations and reconstructed variations in the 1300°C isotherm depth (S5) beneath Greenland, as well as GF variability near its surface (Figure 1). In addition the reconstructed zone of anomalous GF is spatially correlated with highs in the dynamic topography[25] and isostatically compensated bedrock surface (Figure S7), both of which are likely induced by thermal anomalies in the mantle (see Supplementary Information).Our interpretation of the origin of the geothermal anomaly is further supported by evidence of former magmatism found under the present-day ice cover and along the western and eastern margins of Greenland. Mafic dyke fragments recovered from bedrock beneath the GISP2 ice core[26] are similar to basalts from eastern Greenland and there is evidence of large volcanic crater caldera-like formations under the north-central GIS[1]. Together with abundant magmatic rocks from the Greenland margins (Figure 2a), these provide evidence for former volcanic activity in the area of anomalous GF, which may be directly or indirectly plume-related. Taken together, the accumulated evidence indicates that the prominent geothermal anomaly beneath the ice has its origin in the remanent thermal imprint and lithosphere thinning imposed by the plume's residence beneath Greenland tens of millions of years ago. This synopsis of independent evidence supports our earlier hypothesis[16] that the lithosphere thinning beneath the Summit region of the GIS could have resulted from thermal erosion by the Iceland plume.

To date, paleoreconstructions of the Iceland plume history have been marked by a high degree of uncertainty in the location and timing of its residence beneath Greenland, resulting in proposed hotspot tracks located in a 1000-km-wide band from north to south (Figures 2a and S8). A joint interpretation of the geothermal anomaly reconstructed from independent geophysical data (Figure 1) and seismic tomography data (Figures 2a-b) provides new evidence that the Greenland lithosphere passed over the mantle plume several hundred km from the tracks suggested by most existing paleoreconstructions. Of previously proposed plume tracks, the most northerly[9] (Figures 2a and S3) best explains the location of the reconstructed geothermal anomaly. A cursory comparison might suggest that this plume track disagrees with evidence from hotspot-related magmatic rocks at the western margin of Greenland (Figure 2a), where the track reconstruction is less reliable (see Supplementary Information). The degree of disagreement is however hard to judge, since more extensive magmatic sequences supporting this northerly track may be hidden beneath the thick ice cover shielding most of the north-western margin of Greenland (Figure 1). In addition, previous studies have demonstrated that magmatic expression of the plume head at the surface may not necessarily coincide with the position of a plume-feeding conduit[27].

A majority of basal ice melt identified by ice-penetrating radar and ice core measurements[1-4] lies within what we argue to be the area affected by the long-lived thermal and physical imprint of the Iceland plume (Figure 1). The reconstruction of subglacial thermal conditions suggests that about half of the north-central GIS is currently resting on a thawed bed, with extensive melting areas interconnecting fragmentary evidence of basal melt along the flight routes of radar-survey aircraft and at the location of the NGRIP ice core (Figure 3a). In addition we have identified numerous regions such as, for example, in the surroundings of the NEEM ice core, where basal ice is nearly at the pressure-melting point and may contain some meltwater.

High basal melt rates estimated from internal ice layering account for several mm to cm of ice annually lost to melting[1]. Since substantial subglacial lakes are uncommon in Greenland[28], the generated basal meltwater has to be effectively routed towards the ice sheet margins without ponding along the way. A recent subglacial topographic study[3] has suggested potential pathways for drainage of subglacial meltwater, where it may exist, from beneath the GIS. We have compared the topography of this potential drainage system with our reconstructed areas of basal melt and selected for the most likely paths along which the subglacial meltwater must be evacuated (Figure 3a). The overwhelming majority of the previously suggested potential hydrological routes[3] cluster within our predicted basal melt areas, and may be currently active. Furthermore, most of these routes have their headwaters in the zone of the geothermal anomaly. We argue that the combination of enhanced melting, elevated GF, concentration of hydrological pathways, and deeply incised subglacial topography[20] can be explained by the long-lasting imprint of the passage of Greenland over the Iceland mantle plume.

The tectonothermal history is also implicated in the location of development of rapid ice flow in central Greenland. Existing studies attribute the start point of the 750-km-long North-Eastern Greenland Ice Stream (*NEGIS*, Figure 3b) to the influence of high GF and rapid basal melt located at its head[1]. Our study demonstrates that the areas of high GF and basal ice melt inferred from ice-penetrating radar studies[1] and the start point of the NEGIS[5] (Figure 3b) are all located within the reconstructed geothermal anomaly. The elevated GF however is unlikely to be the only factor controlling the observed speed and shape of the NEGIS, which may also be modulated by ice geometrical settings, subglacial hydrology and mechanical properties of the ice-bedrock interface[29].

Our reconstruction of the present-day thermal regime of the GIS reveals more extensive areas of GF-induced basal ice melt than previously recognised[1-4] and makes it possible that a dense network of subglacial meltwater pathways is currently operating beneath the ice, most of which spring from the zone affected by passage over the Iceland plume. Despite the weight of aggregated evidence presented here, it has not previously been hypothesised that the observed melting beneath large sectors of the GIS and anomalous ice streaming in north-eastern

Greenland may be the expression of Iceland hotspot history. The geothermal anomaly provides evidence for a more northerly hotspot track than previously proposed and will offer a useful test for existing paleoreconstructions of absolute plate motion. This study advocates a previously undocumented strong coupling between Greenland's present-day ice dynamics, subglacial hydrology, and the remote tectonothermal history of the North Atlantic region.

## References

[1] Fahnestock, M., Abdalati, W., Joughin, I., Brozena, J. & Gogineni, P. High geothermal heat flow, basal melt, and the origin of rapid ice flow in central Greenland. *Science* **294**, 2338-2342 (2001).

[2] Oswald, G. K. A. & Gogineni, S. P. Mapping basal melt under the northern Greenland ice sheet. *IEEE Trans. Geosci. Rem. Sens.* **50**, 585–592 (2012).

[3] Bell, R. E., Tinto, K., Das, I., Wolovick, M., Chu, W., Creyts, T. T., Frearson, N., Abdi, A., & Paden, J. D. Deformation, warming and softening of Greenland's ice by refreezing meltwater, *Nat. Geosci.* **7**, 497–502 (2014).

[4] Grinsted, A. & Dahl-Jensen, D. A Monte Carlo-tuned model of the flow in the NorthGRIP area. *Ann. Glaciol.* **35**, 527–530 (2002).

[5] Joughin, I, Smith, B. E., Howat, I. M., Scambos, T. & Moon, T. Greenland flow variability from ice-sheet-wide velocity mapping. *J. Glaciol.* **56(197)**, 415–430 (2010).

[6] Rickers, F., Fichtner, A. & Trampert, J. The Iceland—Jan Mayen plume system and its impact on mantle dynamics in the North Atlantic region: evidence from full-waveform inversion. *Earth Planet. Sci. Lett.* **367**, 39-51 (2013).

[7] Jakovlev, A. V., Bushenkova, N. A., Koulakov, I. Y. & Dobretsov, N. L. Structure of the upper mantle in the Circum-Arctic region from regional seismic tomography. *Russ. Geol. Geophys.* **53**, 963_971 (2012).

[8] Doubrovine, P. V., Steinberger, B. & Torsvik, T. H. Absolute plate motions in a reference frame defined by moving hotspots in the Pacific, Atlantic and Indian oceans. *J. Geophys. Res.* **117**, B09101 (2012).

[9] O'Neill, C., Müller, R. D. & Steinberger, B. On the uncertainties in hotspot reconstructions, and the significance of moving hotspot reference frames. *Geochem. Geophys. Geosyst.* **6**, Q04003 (2005).

[10] Schroeder, D. M., Blankenship, D. D., Young, D. A. & Quartini, E.. Evidence for elevated and spatially variable geothermal flux beneath the West Antarctic Ice Sheet. *Proc. Natl. Acad.* Sci. **111(25)**, 9070–9072 (2014).

[11] Kamb, B. Glacier surge mechanism based on linked cavity configuration of the basal water conduit system. *J. Geophys.Res.* **92**(B9), 9083–9100 (1987).

[12] Llubes, M., Lanseau, C. & Remy, F. Relations between basal condition, subglacial hydrological networks and geothermal flux in Antarctica. *Earth Planet. Sci. Lett.* **241**, 655–662 (2006).

[13] Sørensen, L. S. et al. Mass balance of the Greenland ice sheet (2003–2008) from ICESat data – the impact of interpolation, sampling and firn density. *The Cryosphere* **5**, 173-186 (2011).

[14] Parizek, B., Alley, R.B. & Hulbe, C.L. Subglacial thermal balance permits ongoing grounding line retreat along the Siple Coast of West Antarctica. *Annals of Glaciology* **36**, 251-256 (2003).

[15] Artemieva, I. M. Global 1°×1° thermal model TC1 for the continental lithosphere: Implications for lithosphere secular evolution. *Tectonophysics* **416**, 245–277 (2006).

[16] Petrunin, A., Rogozhina, I., Vaughan, A. P. M., Kukkonen, I. T., Kaban, M., Koulakov, I. & Thomas, M. Heat flux variations beneath central Greenland's ice due to anomalously thin lithosphere. *Nature Geosci.* **6**, 746-750 (2013).

[17] Fox Maule, C., Purucker, M. E. & Olsen, N. Inferring Magnetic Crustal Thickness and Geothermal Heat Flux from Crustal Magnetic Field Models (Copenhagen, 2009); available at http://www.dmi.dk/dmi/dkc09-09.pdf.

[18] Kumar, P. *et al.* The lithosphere-asthenosphere boundary in the North-West Atlantic region. *Earth Planet. Sci. Lett.* **236**, 249-257 (2005).

[19] Johnsen, S. J. *et al.* Oxygen isotope and palaeotemperature records from six Greenland ice-core stations: Camp Century, Dye-3, GRIP, GISP2, Renland and NorthGRIP. *J. Quaternary Sci.* **16**, 299–307 (2001).

[20] Bamber, J. L. *et al*. A new bed elevation dataset for Greenland. Cryosphere 7, 499–510 (2013).

[21] Karato, S. Importance of anelasticity in the interpretation of seismic tomography. *Geophys. Res. Lett.* 20, 1623 (1993).

[22] Storey, M., Duncan, R. A., Tegner, C. Timing and duration of volcanism in the North Atlantic Igneous Province: implications for geodynamics and links to the Iceland hotspot. *Chem. Geol.* **241**, 264–281 (2007).

[23] Morgan, W. J. Deep mantle convection plumes and plate motions. *Bull. Am. Assoc. Pet. Geol.* **56**, 203-213 (1972).

[24] Sobolev, S. V. *et al.* Linking mantle plumes, large igneous provinces and environmental catastrophes. *Nature* **477**, 312–316 (2011).

[25] Kaban, M. K., Petrunin, A. G., Schmeling, H. & Shahraki, M. Effect of Decoupling of Lithospheric Plates on the Observed Geoid. Surv. Geophys. 35, 1361–1373 (2014).

[26] Weis, D., Demaiffe, D., Souchez, R., Gow, A. J. & Meese, D. A. Ice sheet development in central Greenland: implications from the Nd, Sr and Pb isotopic compositions of basal material. *Earth Planet. Sci. Lett.* **150**, 161-167 (1997).

[27] Koptev, A., Calais, E., Burov, E., Leroy S. & Gerya, T. Dual continental rift systems generated by plume-lithosphere interaction. *Nat. Geosci.* **8(5)**, 388–392 (2015).

[28] Bamber, J. L., Siegert, M. J., Griggs, J. A., Marshall, S. J. & Spada, G. Paleofluvial Mega-Canyon Beneath the Central Greenland Ice Sheet. *Science* **341 (6149)**, 997-999 (2013).

[29] Kamb, B. Basal zone of theWest Antarctic ice streams and its role in lubrication of their rapid motion. *In* Alley, R.B. and R.A. Bindschadler, *eds. The West Antarctic ice sheet:*

*behavior and environment*. Washington, DC, American Geophysical Union, 157–199 (2001). (Antarctic Research Series 77.)

[30] Henriksen, N., Higgins, A. K., Kalsbeek, F. & Pulvertaft, T. C. R. Greenland from Archaean to Quaternary: Geological map of Greenland, 1:2 500 000. *Geology of Greenland Survey Bulletin* **185**, 93 (2000).

**Acknowledgements**

This study is part of the multinational research initiative IceGeoHeat. We thank Cathrine Fox Maule for sharing the map of Curie depths with us and Winnie Chu and Robin Bell for providing us with their modelled subglacial hydrology network. We also greatly appreciate the suggestions of Alicia Newton, Taras Gerya and two anonymous referees on how to improve the manuscript. This work was partly supported by Netherlands Research Centre for Integrated Solid Earth Sciences, grants ISES-NorMar-2.6 and ISES-UU-PC-cluster, the German Research Foundation, grant PE 2167/1-1, and the Federal Ministry of Education and Research, PalMod project.

**Author contributions**

I.R. developed the concept. I.R. and A.G.P. designed and performed all numerical experiments. I.R and A.P.M.V. wrote the manuscript, with the assistance of A.G.P., B.S. and J.V.J. A.G.P. analyzed the seismic tomography models provided by F.R. and I.K, prepared the map of crustal thickness, assembled the measured GF values from the continental shelf of Greenland and prepared and described the materials related to the model setup and thermal state of the Greenland lithosphere. B.S. prepared and described the materials related to existing plume track reconstructions and contributed to the design of Supplementary Information. J.V.J. tested the GF map using his high-resolution Greenland ice sheet model VarGlaS. M.K.K. performed the analysis of the observed gravity data. All authors contributed to discussions and interpretations of the results.

**Additional information**

The authors declare no competing financial interests.

## Code and data availability

All data and the components of the coupled 3-D ice sheet-lithosphere model are available in a digital form upon request (irogozhina@marum.de).

## Corresponding author

Correspondence and requests for materials should be addressed to Irina Rogozhina (irogozhina@marum.de)

## Figure captions

**Fig. 1.** Predicted GF [$mW/m^2$] at 5 km depth below bedrock surface. GF was corrected for crustal heat production using a parameterization of radiogenic heat sources (see Methods). Modeled thermal state of the GIS and lithosphere calibrated by in-situ data shown by orange/black triangles (filled - ice cores, unfilled - bedrock borehole measurements) and black/white crosses[1,4], diamonds[2] and stars[3] (basal melting from radar and ice core measurements). Deep ice core locations[19]: CC, NEEM, NGRIP, GRIP, GISP2 and Dye3. Measured basal ice temperatures and GF from bedrock boreholes (1-7) presented in Tables S4-S5. White curves outline ice sheet and coastal margins.

**Fig. 2.** Geophysical data indicating lithosphere anomalies beneath Greenland. a) S-wave velocity model of the North Atlantic region[5] shown for the Greenland region at 120 km depth[5], colour-mapped for percentage velocity anomaly. Areas of hotspot-related magmatism are hatched and labeled for age[30]. Iceland hotspot track reconstructions[8-9] are shown as continuous lines for 0-60 Ma and dashed lines prior to 60 Ma (see Figure S8 caption). b) P-wave velocity model of the circum-Arctic region[7] shown for north-central Greenland at 150 km depth, colour-mapped for percentage velocity anomaly. Black and orange triangles mark ice core and bedrock borehole locations as in Figure 1.

**Fig. 3.** Predicted basal thermal state of the present-day GIS. a) Modeled basal ice temperature below the pressure-melting point [ºC], with superimposed potential active hydrological routes adopted from a subglacial topographic study[3] (red curves, see Full Methods, M2). Areas coloured white are where our model predicted melting at ice sheet base. Triangles mark ice core locations. b) The reconstructed geothermal anomaly (contours) superimposed on the observed surface ice velocity[5] (colour-mapped) of the north-eastern GIS [m/a] shows that the head of the North-Eastern Greenland Ice Stream (labeled by NEGIS) is located in the area of the highest GF values (above 90 $mW/m^2$).

## Methods

*M1. Model description and forcing*

**Description:** Our modelling strategy uses a 3-D fully coupled thermomechanical model of the GIS and the lithosphere[16]. The ice component is implemented using the 3-D finite-difference ice sheet model (ISM) SICOPOLIS based on the shallow ice approximation and the rheology of an incompressible, heat-conducting, power-law fluid described by Glen's flow law[31]. Numerical solutions of mass, momentum and energy balance equations describe ice dynamics and thermal evolution of the GIS. The model is polythermal and allows formation of temperate ice at the ice sheet's base, overlain by a thick layer of cold ice. Mass- and energy-flux conditions at the interface between cold and temperate ice are realized through the solution of the Stefan problem[31]. Surface melting and refreezing are calculated using a temperature index[32] and a meltwater retention[33] methods. Basal sliding is described by a Weertman-type sliding law[34]. The parameters of the ISM (Table S1) were calibrated using an iterative approach described in Section M2 to attain the best possible fit with the observed ice thickness. The lithospheric model is implemented using the 3-D finite-volume thermo-mechanical code Lapex 3D[35-36] incorporating a non-linear temperature- and stress-dependent visco-elasto-plastic rheology with parameters consistent with laboratory measurements (Table S2). The lithosphere model includes the upper and lower crust and the lithospheric mantle and adopts a pressure-temperature-dependent law for thermal diffusivity in both the lithospheric mantle and the crust[37]. The bedrock surface is constructed using the most recent compilation of ice-penetrating radar measurements[20]. The thickness of the crust across north-central Greenland is based on CRUST1.0[38], regionally adjusted to fit the estimates from S-receiver functions[39] and gravity data[40]. The crust is subdivided into two parts of equal thickness with different thermal properties: the felsic crust with higher radiogenic production and the mafic crust with lower radiogenic production[41]. Here we employ a uniform distribution of radioactive elements within the upper crust, and mean crustal heat production of 0.3 μW/m$^3$ estimated in our previous study for central Greenland[16] in agreement with bedrock borehole measurements from western Greenland[16,42]. Our previous studies[16,35-36,43] describe the 3-D ice sheet and lithosphere model components in more detail.

**Boundary conditions:** The ice sheet and lithosphere components are coupled through boundary conditions, requiring continuity of internal energy and normal stress at the exchange boundary[16] using the methodology of Greve[31]. The hydrostatic pressure at the base of the ice sheet is transmitted to the lithospheric model as a loading that produces a dynamic response in the lithosphere. The resulting surface subsidence or uplift is then passed back to the ISM as a correction to the bedrock topography.

The lower boundary of the thermal lithosphere is defined as the depth where the asthenospheric potential temperature reaches 1300ºC[15]. The Winkler boundary condition that implies zero viscous drag forces and hydrostatic normal-to-surface stress is prescribed at the lower boundary of the model box. Free slip boundary conditions (the normal-to-boundary component of velocity vector is equal to zero) are set for the upper 50 km at the side boundaries, whereas the remaining boundaries are open for in-out flow. No conductive heat exchange is allowed at these boundaries, i.e., the thermal gradient is equal to zero.

The coupled model is driven from above by time-evolved temperature and precipitation forcing over the period of large-scale glaciations in Greenland, which are assumed to have initiated in the Mid-Pliocene[44]. Climate history is inferred using an empirical relation[45] to combine surface temperature records from ice cores with precipitation. The air temperature forcing uses the combined GRIP-EPICA surface temperature record[16,45-46] applied as a time-varying spatially uniform offset from the present-day air temperature distribution across Greenland, corrected for the monthly lapse rates inferred from in-situ measurements[47]. The precipitation field across Greenland is derived at each time step by applying a scaling to the present-day precipitation rate[48] depending on the temperature offset relative to the present. The global sea level forcing is derived from the SPECMAP marine $\delta^{18}O$ record[49]. Prior to the onset of large-scale glaciations 3 Ma, we initialize the Greenland lithosphere model to a thermal equilibrium with a surface temperature of 0˚C[44] at the ice-free upper boundary. The components of the coupled model together with their boundary conditions are schematically illustrated in Figure S1.

**Discretization**: Simulations are performed with a horizontal resolution of 10 km. The ISM and the thermal component of the lithospheric model are run with a time step of 1 year, whereas the mechanical component of the lithospheric model uses a time step of 100 years. The vertical resolution is non-uniform and provides grid densification towards the ice-bedrock interface in both lithosphere and ice sheet model components. Computational grids adopted by the SICOPOLIS and Lapex 3D codes coincide at the interface surface (in the nodes where temperature is evaluated). The vertical grids within cold-ice and temperate-ice columns include 81 and 11 points, respectively[50]. Vertical resolution of the lithospheric model component is 1 km in the upper crust and 5 km below. Temperature distribution within the upper 5 km of the crust is calculated on a fine sub-mesh including 161 vertical grid points densifying towards the lithosphere surface.

*M2. Model calibration*

Throughout the modelling procedure we apply a multi-step calibration of the ice-lithosphere model against magnetic and seismic data, observations of the present-day GIS and GF estimates from the bedrock temperature measurements (see section M3). Major steps of model calibration are schematically shown in Figure S2.

**Stage I**: The 1300ºC isotherm depth is first derived from a 1-D model of ice and lithosphere[16] using the Curie depths (580ºC) from satellite magnetic data[17] and seismic lithosphere thickness from S-receiver functions[18,51] as constraints. The resulting non-linear evolution equation for vertical advection and diffusion is solved with finite differences, using the procedure described in our previous study[16]. The thickness and structure of the crust are taken to be identical to those adopted by the 3-D ice-lithosphere model (see Section M1).

**Stage II**: The preliminary map of the 1300ºC isotherm depth obtained from Stage I is then used to define a lower thermal boundary in a 3-D GIS-lithosphere model. From a reference simulation of the GIS-lithosphere history spanning 3 million years we estimate the deviations from the observed present-day ice thickness[20] and balance ice velocity[52]. As a result we also derive the states of the GIS and lithosphere for the time slice corresponding to 100 ka, which are then used as initial conditions at Stage III[53].

**Stage III**: We run a suite of simulations starting from the initial condition (100 ka) to select general parameters of the ISM (basal sliding coefficient, ice flow enhancement factors, degree-day factors for snow and ice, daily temperature standard deviation and temperature-dependent snow-rain fractionation of precipitation) in order to achieve the best possible fit with the observed present-day ice sheet thickness[20] and balance velocity[52] and to derive our intermediate maps of GF distribution and basal ice temperatures across north-central Greenland. At this stage we calibrate the GIS model component using an adaptive random search algorithm developed for optimization of nonlinear systems with many parameters[54-55]. To reduce the computation time, main stages of the process have been parallelized following a strategy applied to the parameter search using coupled simulations with increasing horizontal (10-20 km) and temporal (1-10 years) resolution, thereby gradually narrowing permissible regions for each parameter. Here we use the following objective function to measure the goodness of the fit of the ice thickness and surface speed to the observations:

$$J(\alpha) = \sqrt{W_H S_H + W_v S_v}, \tag{1}$$

where $S_H = \sum_{H_{obs}(x,y) \geq H_{thresh}} \left(1 - \frac{H(x,y)}{H_{obs}(x,y)}\right)^2$, (2)

$$S_v = \sum_{H_{obs}(x,y)\geq H_{thresh}} \left(1 - \frac{v(x,y)}{v_{obs}(x,y)}\right)^2 , \tag{3}$$

where $H(x, y)$ and $H_{obs}(x, y)$ are the computed and observed ice thickness, and $v(x,y)$ and $v_{obs}(x,y)$ are computed and balance ice speed, respectively.

The fit is only evaluated where the present-day ice thickness exceeds 1.5 km ($H_{thresh}$ = 1.5 km), since the focus of this study is on the inland areas where GF is one of the major factors shaping subglacial thermal conditions. In addition this results in a minimal influence of the deficiencies of the shallow ice approximation on our choice of the general parameters of the ISM component[56]. Due to higher significance of the fit between the modelled and observed ice thickness for the reconstruction of basal ice temperatures in the targeted areas, unequal weights of $W_H$ = 0.78 and $W_v$ = 0.22 have been empirically chosen for calibration.

Using this approach we calibrate model parameters that have the strongest influence on the modelled present-day ice thickness and ice flow pattern. Here we refrain from making assumptions about spatial variability in such parameters as basal sliding coefficients and ice flow enhancement factors, since observational data are currently insufficient to support such assumptions. We therefore search for the best-fit single values of relevant parameters within the ranges adopted from existing literature that are commonly applied to the modelling of the large-scale characteristics of the GIS. The only exception is the daily temperature standard deviation parameter in a temperature-index method, which has recently been reported highly variable across Greenland[57-58] and strongly dependent on variations in surface temperature[59-60]. We have tested the performance of the two existing temperature-dependent parameterizations of daily temperature standard deviation[59-60] and concluded that the use of the latter parameterization[60] over the Holocene period yields better results for the present-day GIS thickness. Since the existing temperature-dependent parameterizations of daily temperature standard deviation are inferred from the present-day observations and their applicability to glacial periods has not yet been demonstrated, our calibration strategy includes the search of a best-fit daily temperature standard deviation parameter in the period prior to the Holocene interglacial within the range of previously reported constant values. The ranges of tested parameter values (initial permissible regions) are provided in Table S3.

**Stage IV:** After the calibration of the modelled ice thickness and ice velocity we evaluate the agreement between the model and available direct constraints from the ice sheet and bedrock (GF and ice core temperature measurements, basal melt locations from radar soundings, and inland regions of high ice velocity, see Figure 1 and Tables S4 and S5) and outline the locations/areas that require corrections to the GF estimates. Again, we only use those constraints from the ice sheet that fall within the area with the present-day ice thickness above 1.5 km, for which the ISM parameters are calibrated at Stage III. In particular, this is done to exclude observational data falling within the zones where surface meltwater delivery to the ice sheet bed[61] and ocean-induced variations in glacier dynamics and subglacial hydrology[62] may have significant effects on the basal thermal regime of the present-day GIS. For the areas where the dynamic features are poorly captured after the calibration procedure at Stage III, we apply a fairly restrictive tuning method. In such areas local adjustments of the initial 1300ºC-isotherm depth are limited to a maximum correction of ± 15% to the modelled Curie depth, which is within the range of anticipated errors in the estimates from the satellite magnetic data[63] (see M3). Due to the diverse nature of available constraining data, the calibration process could not be fully automated. Across ice-covered areas, we have set up a correspondence between each direct constraint from the ice sheet and the modelled horizontal ice velocity within the grid cell where the constraint is located. For GF measurements from the bedrock the velocity value has been set to zero. The constraints have been sorted according to the corresponding velocity value in order to account for the growing influence of the horizontal advection on the thermal regime of the neighbouring areas towards the ice sheet margins. The calibration has therefore been organized starting from data points with minimal velocity values.

The GF estimates derived from Stage III are adjusted to fit observations over each outlined area through successive perturbations to the preliminary map of the 1300ºC isotherm depth from Stage II leading to local increases/decreases in subglacial heat flow, modelled basal ice temperature and vertical temperature gradients. The perturbations are performed across the neighbourhood of each data point representative of the resolution of the magnetic data[17] used at Stage I (see M3). Following a simple under-relaxation procedure, only a fraction of the correction value necessary to fit each individual constraint is retained, depending on the ice flow velocity value within the grid cell where the correction was estimated:

$$H_n^L(x,y) = H_{n-1}^L(x,y) + \alpha\left(H_n^{L*}(x,y) - H_{n-1}^L(x,y)\right), \quad (4)$$

where $\alpha = (1 - \frac{v(x,y)}{2v_{max}})$, $v_{max}$ is the maximum absolute value of the horizontal ice flow velocity in the areas subject to corrections, and $H_n^{L*}(x,y)$ and $H_{n-1}^L(x,y)$ indicate the 1300ºC isotherm depths, which are estimated to fit the surface constraint for the iteration $n$ and obtained from the previous iteration ($n$-1), respectively.

Overlapping corrections are combined using a weighted average, with the weights inversely proportional to the distances to the locations of the constraining data. The correction map is then smoothed using a low-pass filter. Stages II – IV are repeated until the process converges to the best-fit solution with all constraints using updated maps of 1300ºC isotherm depths within individual threshold values established for each type of constraint.

The final series of simulations is run in order to introduce final adjustments at the locations where the smoothing procedure, or interference between perturbations over neighbouring areas, affected the fit with observations.

**Stage V**: At the last stage we infer the potential subglacial hydrology beneath the north-central GIS from the hydrology network calculated by [ref. 3] using the hydraulic potential equation of [ref. 64] and the approach of [ref. 65] for routing subglacial meltwater over the hydraulic potential surface. We have superimposed these potential hydrological routes on the reconstructed basal ice temperature of the present-day GIS. Among them, the routes that fall within the areas of predicted basal ice melting have been selected as the most probable routes of currently active subglacial hydrology (shown by solid red curves in Figure 3a). We have also retained the potential hydrological routes that fall within the areas with the ice base close to the pressure-melting point (dashed red curves in Figure 3A) where the presence of meltwater is probable but may not be retrieved by our model due to insufficient horizontal resolution (see M1) that acts as a filter of high-frequency signals present in the original bedrock topography data set[20].

*M3. Description of model constraints*

At Stage I we use estimates of Curie depths[17] from satellite magnetic data and lithosphere thickness from seismic data[18,51] to derive our initial 1300ºC isotherm depths. The Curie depth map was inferred with a horizontal resolution of a few hundred km and an uncertainty of about ±15%[63]. The estimates of seismic lithosphere thickness are provided as average values over eight areas of variable size[18] and along S-N profiles in central Greenland[51]. Most of the average values are derived across the areas with the dimensions of about 500 km (S-N direction) by 200 km (W-E direction).

At Stage III the model is calibrated versus ice thickness from radar soundings[20] and balance ice velocity[52]. Ice thickness is provided with a horizontal resolution of 1 km (Figure S3), although this resolution may not locally be reached due to uneven distribution of radar measurements across Greenland[20]. The uncertainty in the observed ice thickness mostly exceeds 100 m, with the highest uncertainty of more than 150 m occurring in East Greenland and along the GIS margin[20]. Following the approach described in [ref. 52], we determine balance velocity by minimizing the difference between balance and observed surface speed, using accumulation and its associated uncertainty as a control variable. Its distribution is given on an unstructured grid densifying towards the areas of rapid flow, with an average horizontal resolution of 2 km. Balance, rather than observed velocity is used for its continuity around the ice divide and lack of noise in regions of low speed. To enable a one-to-one comparison between the modeled and observed fields, we have smoothed the observational fields by assigning an average value to each model grid cell.

At Stage IV we calibrate our model versus in-situ measurements of basal ice temperature and GF and basal ice melt from radar soundings. The uncertainties in ice core measurements are low (e.g., 0.0045°C for GISP2[66]), whereas GF estimates are likely less reliable, since most of the GF values have been derived from relatively shallow boreholes (<1 km depth) and have not been corrected for paleoclimate signal[42,67-68]. To constrain the areas of melting beneath the GIS we use three datasets derived from ice-penetrating radar measurements[1-3] (schematically shown in Figure 1). The first dataset[1] comprises estimates of melt rates beneath the north-central GIS from an interpretation of the internal ice layering. To date, this is the only dataset that includes quantitative analysis of basal melt rates across a large sector in Greenland. The estimated rates may be corrupted by the assumption of equilibrated climate conditions and simplified treatment of the horizontal flow[1] but the inference of basal melt locations is relatively robust. The second dataset[2] hypothesizes the presence of subglacial water based on an empirical relation between relative reflection intensity and thawed/frozen interfaces[69]. Comparison of the first and second datasets across the area included in both studies reveals comparable large-scale patterns of basal melt, with local discrepancies in the predicted melt locations. This may be partly explained by high sensitivity of the method used in the second study to the uncertainties in the bed roughness[2,69]. In addition, the empirical relation uses a somewhat arbitrary threshold to distinguish between melting and frozen areas. Indeed, the authors admit that their inferred subglacial meltwater is not always consistent with ice core measurements (for example, subglacial meltwater is found in the vicinity of the Camp Century (CC) ice core where basal temperature of -13°C has been measured, see Table S4). The third dataset[3] is based on an analysis of the reflections in the radar soundings used to detect basal units of refrozen meltwater, which can be indirectly linked to subglacial melting in the vicinity of these areas. Although the exact locations of subglacial melt cannot be directly inferred from this dataset, here we assume that the identified basal units are situated in a close proximity to the hypothesized subglacial melt (within the same grid cell). Over the overlapping areas we assign higher weights to the constraints from the first dataset.

**References (Methods):**

[31] Greve, R. A continuum-mechanical formulation for shallow polythermal ice sheets. *Philos. Trans. R. Soc. Lond. Ser.* **A355**, 921-974 (1997).

[32] Hock, R. Temperature index melt modelling in mountain areas, *J. Hydrol.* **282**(1-4), 104-115 (2003).

[33] Janssens, I. & Huybrechts, P. The treatment of meltwater retention in mass-balance parameterisations of the Greenland ice sheet, *Ann. Glaciol.* **31**, 133–140 (2000).

[34] Hindmarsh, R.C.A. & Le Meur, E. Dynamical processes involved in the retreat of marine ice sheets. *J. Glaciol.* **47**(157), 271–282 (2001).

[35] Petrunin, A. G. & Sobolev, S. V. Three-dimensional numerical models of the evolution of pull-apart basins. *Phys. Earth Planet. Inter.* **171**, 387–399 (2008).

[36] Petrunin, A. G. & Sobolev, S. V. What controls thickness of sediments and lithospheric deformation at a pull-apart basin? *Geology* **34**, 389 (2006).

[37] Förster, H.-J., Förster, A., Oberhänsli, R. & Stromeyer, D. Lithospheric composition and thermal structure of the Arabian Shield in Jordan. *Tectonophysics* **481**, 29–37 (2010).

[38] Laske, G., Masters., G., Ma, Z. & Pasyanos, M. Update on CRUST1.0 - A 1-degree Global Model of Earth's Crust. *Geophys. Res. Abstracts* **15**, Abstract EGU2013-2658 (2013).

[39] Kumar, P., Kind, R., Priestley, K. & Dahl-Jensen, T. Crustal structure of Iceland and Greenland from receiver function studies. *J. Geophys. Res.* **112**, B03301 (2007).

[40] Braun, A., Kim, H., Csatho, B. & Vonfrese, R. Gravity-inferred crustal thickness of Greenland. *Earth Planet. Sci. Lett.* **262(1-2)**, 138–158 (2007).

[41] Mareschal, J.-C. & Jaupart, C. Radiogenic heat production, thermal regime and evolution of continental crust. *Tectonophysics* **609**, 524-534 (2013).

[42] Harper, J. *et al.* The Greenland Analogue Project report (Olkiluoto, 2012); available at http://www.posiva.fi/files/2826/WR_2012-16web.pdf.

[43] Rogozhina, I. *et al.* Effects of uncertainties in the geothermal heat flux distribution on the Greenland Ice Sheet: An assessment of existing heat flow models. *J. Geophys. Res.* **117**, F02025 (2012).

[44] Brouwers, E. M., Jørgensen, N. O. & Cronin, T. M. Climatic significance of the ostracode fauna from the Pliocene Kap København Formation, north Greenland. *Micropaleontology* **37**, 245-267 (1991).

[45] Dahl-Jensen, D. *et al.* Past temperatures directly from the Greenland Ice Sheet. *Science* **282**, 268-271 (1998).

[46] Augustin, L. *et al.* Eight glacial cycles from an Antarctic ice core. *Nature* **429**, 623-628 (2004).

[47] Fausto, R. S., Ahlstrøm, A. P., Van As, D., Bøggild, C. E. & Johnsen, S. J. A new present-day temperature parameterization for Greenland. *J. Glaciol.* **55**, 11 (2009).

[48] Ettema, J. *et al.* Higher surface mass balance of the Greenland ice sheet revealed by high-resolution climate modeling. *Geophys. Res. Lett.* **36(12)**, 1–5 (2009).

[49] Imbrie, J. Z. *et al*. The orbital theory of Pleistocene climate: Support from a revised chronology of the marine d18O record, in Milankovitch and Climate: Understanding the Response to Astronomical Forcing. Part 1, edited by A. Berger et al., pp. 269–305, D. Reidel, Dordrecht, Netherlands (1984).

[50] Greve, R. Application of a polythermal three-dimensional ice sheet model to the Greenland ice sheet: response to steady-state and transient climate scenarios. *J. Clim*. **10** (1997), 901–918 (1997).

[51] Darbyshire, F. A. *et al.* A first detailed look at the Greenland lithosphere and upper mantle, using Rayleigh wave tomography. *Geophys. J. Int.* **158**, 267–286 (2004).

[52] Brinkerhoff, D. & Johnson, J. A stabilized finite element method for calculating balance velocities in ice sheets. *Geosci. Model Dev.* **8**, 1275 – 1283 (2015).

[53] Rogozhina, I., Martinec, Z., Hagedoorn, J. M., Thomas, M. & Fleming, K. On the long-term memory of the Greenland Ice Sheet. *J. Geophys. Res.* **116**, F01011 (2011).

[54] Masri, S. F., Bekey, G. A. & Safford, F. B. A global optimization algorithm using adaptive random search. *Applied Math. and Computation* **7**, 353 (1980).

[55] Bekey, G. A. & Masri, S. F. Random search techniques for optimization of nonlinear systems with many parameters. *Mathematics and Computers in Simulation XXV*, 210 - 213 (1983).

[56] Bueler, E., Lingle, C. S., Kallen-Brown, J. A., Covey, D. N. & Bowman, L. N. Exact solutions and verification of numerical models for isothermal ice sheets. *J. Glaciol.* **51**, 291–306 (2005).

[57] Fausto, R. S., Ahlstrøm, A. P., van As, D. & Steffen, K. Present-day temperature standard deviation parameterization for Greenland. *J. Glaciol.* 57, 1181–1183 (2011).

[58] Rogozhina, I. & Rau, D.. Vital role of daily temperature variability in surface mass balance parameterizations of the Greenland Ice Sheet. *The Cryosphere* **8**, 575-585 (2014).

[59] Wake, L. M. & Marshall, S. J. Assessment of current methods of positive degree-day calculation using in situ observations from glaciated areas. *J. Glaciol.* **61**(226), 329-344 (2015).

[60] Seguinot, J. & Rogozhina, I. Daily temperature variability predetermined by thermal conditions over ice-sheet surfaces. *J. Glaciol.*, **60**(221), 603–605 (2014).

[61] Clason, C. C. *et al.* Modelling the transfer of supraglacial meltwater to the bed of Leverett Glacier, Southwest Greenland. *The Cryosphere* **9**, 123 - 138 (2015).

[62] Straneo, F. & Heimbach, P. North Atlantic warming and the retreat of Greenland's outlet glaciers. *Nature* **504**, 36 -43 (2013)

[63] Fox Maule, C., Purucker, M. E., Olsen, N. & Mosegaard, K. Heat flux anomalies in Antarctica revealed by satellite magnetic data. *Science* **309**, 464-467 (2005).

[64] Shreve, R. L. Movement of water in glaciers. *J. Glaciol.* **11** (62), 205-214 (1972).

[65] Flowers, G. E. & Clarke, G. K. C. Surface and bed topography of Trapridge Glacier, Yukon Territory, Canada: digital elevation models and derived hydraulic geometry. *J. Glaciol.* **45,** 165_174 (1999).

[66] Cuffey, K. M. *et al.* Large Arctic Temperature Change at the Wisconsin-Holocene Glacial Transition. *Science* **270**, 455–458 (1995).

[67] Sass, J. H., B. L. Nielsen, H. A. Wollenberg, and R. J. Munroe. Heat flow and surface radioactivity at two sites in South Greenland. *J. Geophys. Res.* **77**, 6435–6444 (1972).

[68] Balling, N. & Brooks, C.K. Heat flow measurements in the Skaregaard Intrusion – A progress report (Copenhagen, 1991). Proceedings of a meeting held on January 1991 in the Geological Institute, University of Copenhagen: Kangerdlugssuag studies. Processes at a rifted continental margin. Ed. C.K. Brooks and T. Stærmose.

[69] Oswald, G. & Gogineni, S. Recovery of subglacial water extent from Greenland radar survey data. *J. Glaciol.* **54**, 94–106 (2008).

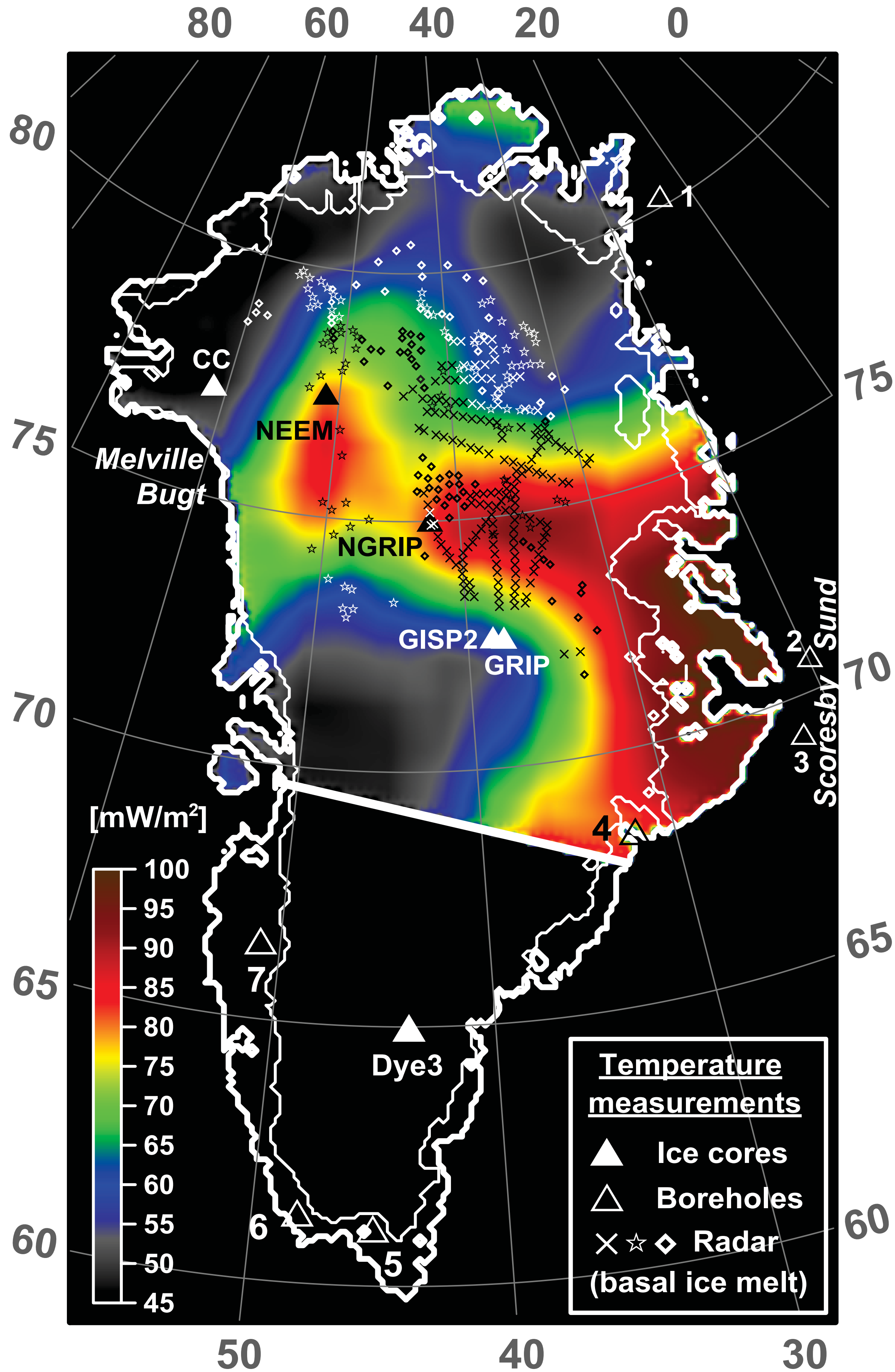
80
60
40
20
0
80
75
70
65
60
75
70
65
60
50
40
30
1
CC
NEEM
Melville
Bugt
NGRIP
GISP2
GRIP
2
3
Scoresby Sund
4
[mW/m²]
100
95
90
85
80
75
70
65
60
55
50
45
7
Dye3
6
5
Temperature
measurements
Ice cores
Boreholes
Radar
(basal ice melt)

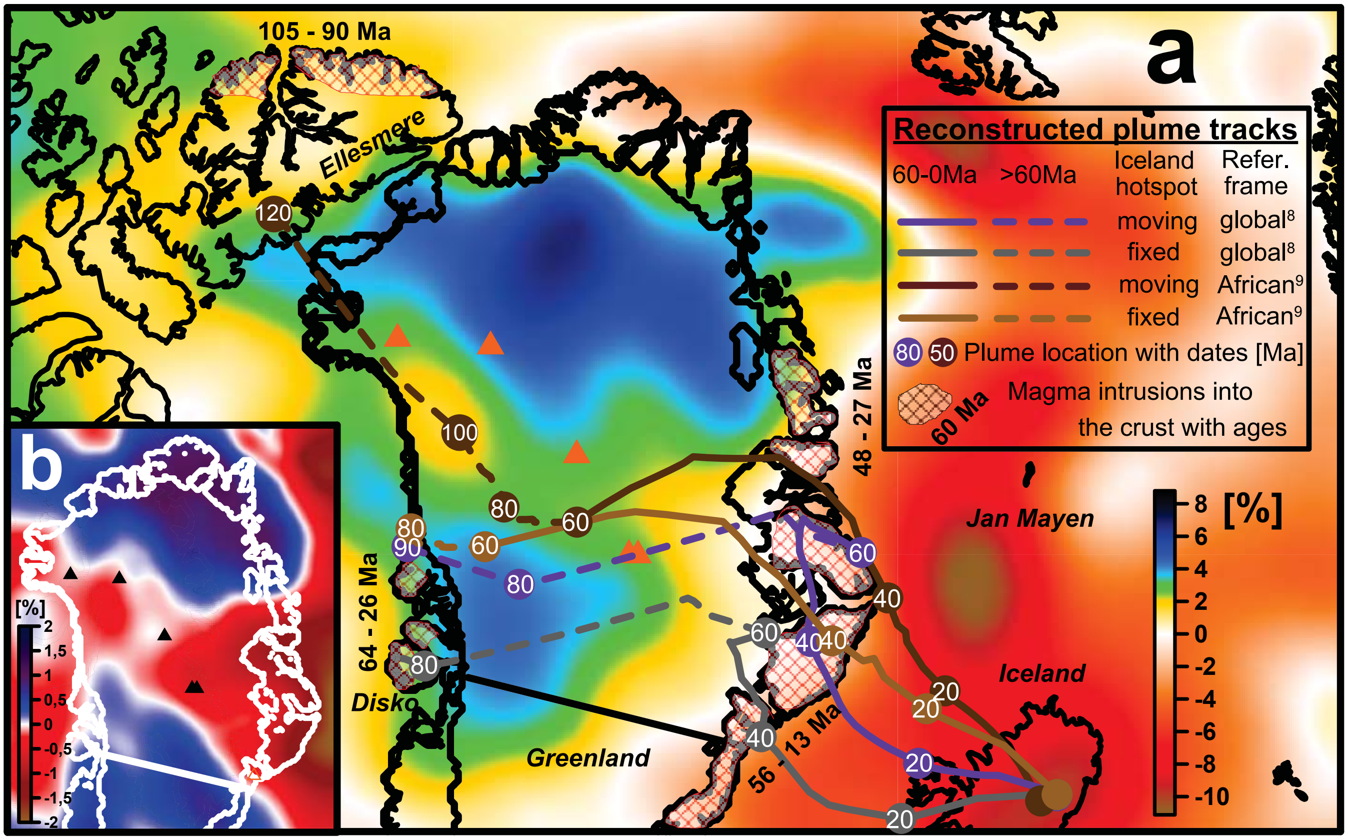

a
105 - 90 Ma
Ellesmere
Reconstructed plume tracks
60-0Ma
>60Ma
Iceland hotspot
Refer. frame
moving
global8
fixed
global8
moving
African9
fixed
African9
80 50 Plume location with dates [Ma]
Magma intrusions into the crust with ages
60 Ma
48 - 27 Ma
64 - 26 Ma
56 - 13 Ma
Jan Mayen
Iceland
Greenland
Disko
[%]
b

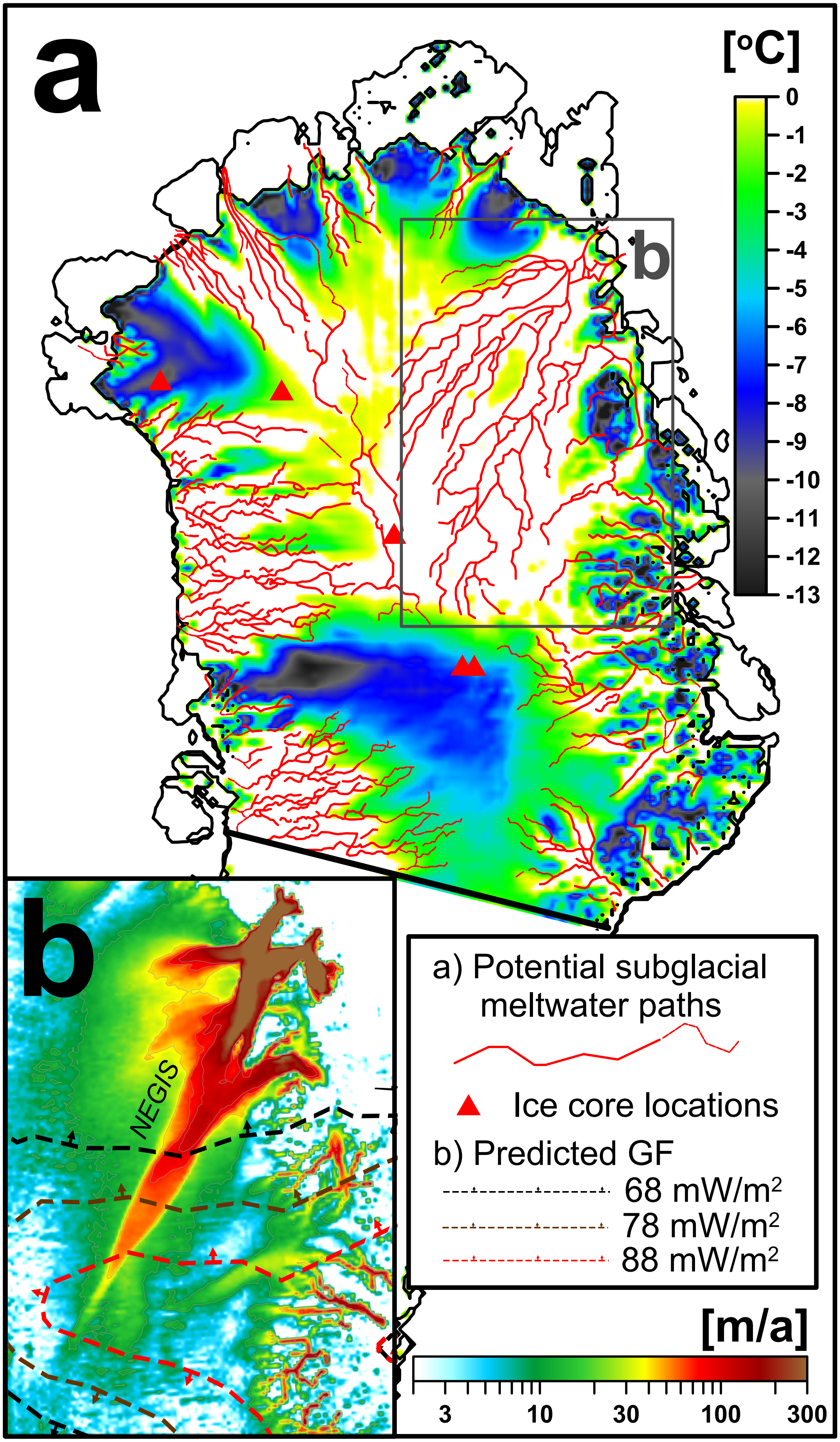
a
[°C]
0
-1
-2
-3
-4
-5
-6
-7
-8
-9
-10
-11
-12
-13
b
b
NEGIS
a) Potential subglacial meltwater paths
Ice core locations
b) Predicted GF
68 mW/m²
78 mW/m²
88 mW/m²
[m/a]
3
10
30
100
300